Alterations in the Arf6-regulated plasma membrane endosomal recycling pathway in cells overexpressing the tetraspan protein Gas3/PMP22

Romina Chies[1,5], Lucilla Nobbio[4], Paolo Edomi[3], Angelo Schenone[4], Claudio Schneider[1,2] and Claudio Brancolini[1,5,*]

[1]Dipartimento di Scienze e Tecnologie Biomediche, Sezione di Biologia, Universita' di Udine, P.le Kolbe 4, 33100 Udine, Italy
[2]Laboratorio Nazionale Consorzio Interuniversitario Biotecnologie AREA Science Park, Padriciano 99, 34142 Trieste, Italy
[3]Dipartimento di Biologia, Universita' di Trieste, v. Giorgieri 5, 34100 Trieste, Italy
[4]Dipartimento di Scienze Neurologiche e della Visione Universita' di Genova, v. dei Toni 5, 16138 Genova, Italy
[5]MATI Center of Excellence, Universita' di Udine, P.le Kolbe 4, 33100 Udine, Italy
*Author for correspondence (e-mail: cbrancolini@makek.dstb.uniud.it)

Accepted 17 December 2002
Journal of Cell Science 116, 987-999 © 2003 The Company of Biologists Ltd
doi:10.1242/jcs.00326

Summary

Growth arrest specific 3 (Gas3)/peripheral myelin protein 22 (PMP22) is a component of the compact peripheral nerve myelin, and mutations affecting *gas3/PMP22* gene are responsible for a group of peripheral neuropathies in humans. We have performed in vivo imaging in order to investigate in detail the phenotype induced by Gas3/PMP22 overexpression in cultured cells. Here we show that Gas3/PMP22 triggers the accumulation of vacuoles, before the induction of cell death or of changes in cell spreading. Overexpressed Gas3/PMP22 accumulates into two distinct types of intracellular membrane compartments. Gas3/PMP2 accumulates within late endosomes close to the juxtanuclear region, whereas in the proximity of the cell periphery, it induces the formation of actin/phosphatidylinositol (4,5)-bisphosphate (PIP_2)-positive large vacuoles. Gas3/PMP22-induced vacuoles do not contain transferrin receptor, but instead they trap membrane proteins that normally traffic through the ADP-ribosylation factor 6 (Arf6) endosomal compartment. Arf6 and Arf6-Q67L co-localize with Gas3/PMP22 in these vacuoles, and the dominant negative mutant of Arf6, T27N, blocks the appearance of vacuoles in response to Gas3/PMP22, but not its accumulation in the late endosomes. Finally a point mutant of Gas3/PMP22 responsible for the Charcot-Marie-Tooth 1A disease is unable to trigger the accumulation of PIP_2-positive vacuoles. Altogether these results suggest that increased Gas3/PMP22 levels can alter membrane traffic of the Arf6 plasma-membrane–endosomal recycling pathway and show that, similarly to other tetraspan proteins, Gas3/PMP22 can accumulate in the late endosomes.

Key words: Tetraspan proteins, Peripheral neuropathies, Schwann cells, Myelin, PIP_2

Introduction

Growth arrest specific 3 (Gas3)/peripheral myelin protein 22 (PMP22) is a glycoprotein highly expressed in Schwann cells (SCs), where it localizes to the compact myelin. Gas3/PMP22 belongs to a family of membrane proteins characterized by the presence of four putative transmembrane domains (Attardi et al., 2000; Bronstein, 2000). Gas3/PMP22 is expressed at high levels in Schwann cells, where it accounts for 2-5% of total myelin proteins (Spreyer et al., 1991; Welcher et al., 1991; Snipes et al., 1992), and at low levels outside the peripheral nervous system (Suter et al., 1994; Baechner et al., 1995; Fabbretti et al., 1995; Notterpek et al., 2001).

Different genetic studies in humans and mice have established a critical role of Gas3/PMP22 in regulating myelin stability/formation (Naef and Suter, 1998). Deletions, duplications and mutations in *Gas3/PMP22* account for the majority of heritable demyelinating peripheral neuropathies. Genomic duplication on 17p11.2-p12, containing the *gas3/PMP22* locus, causes the Charcot-Marie-Tooth type 1A (CMT1A) disease, a peripheral neuropathy that results in progressive distal muscle atrophy and impaired sensation of the limbs (Patel and Lupski, 1994; Suter and Snipes, 1995; Hanemann and Muller, 1998). Nerve biopsies from CMT1A patients mark signs of demyelination and remyelination indicated by redundant Schwann cell processes forming onion bulbs (Suter and Snipes, 1995).

Various mouse and rat models have been generated in an attempt to reproduce the effect of PMP22 overexpression seen in CMT1A (Huxley et al., 1996; Magyar et al., 1995; Sereda et al., 1996; Perea et al., 2001). These animals show a severe demyelination and peripheral neuropathy, and have allowed a more detailed description of the pathogenic events induced by Gas3/PMP22 overexpression. Electron microscopy studies of the sciatic nerves from these transgenic mice showed evidence of severe disruption of myelin formation and sometimes Schwann cells contain myelin debris, products of abnormal myelin assembly and other vesicular structures (Niemann et al., 2000).

Despite the plethora of studies confirming the critical role of Gas3/PMP22 in peripheral neuropathies, the mechanism

through which it can regulate membrane stability is still undefined. Overexpression studies in cultured cells suggest that Gas3/PMP22 can regulate cell cycle (Zoidl et al., 1995), apoptosis (Fabbretti et al., 1995; Zoidl et al., 1997) and cell spreading/adhesion (Brancolini et al., 1999; Notterpek et al., 2001), but here again it is still unclear whether these responses are critical for myelin stability.

Imaging of live cells is the strategy of choice to understand how specific proteins can modulate dynamic changes at the cell surface. To gain more insight into the mechanisms responsible for the demyelination effect of Gas3/PMP22 we have generated a Gas3/PMP22-GFP fusion protein to observe in vivo the cellular response to Gas3/PMP22 overexpression.

The time-lapse analysis has shown that Gas3/PMP22, before triggering changes in cell spreading/survival, induces the accumulation of intracellular vacuoles. Our studies demonstrate that overexpressed Gas3/PMP22 accumulates into two distinct intracellular membrane compartments. Gas3/PMP22 aggregates within late endosomes close to the juxtanuclear region, whereas in the proximity of the cell periphery it induces the formation of actin/phosphatidylinositol (4,5)-bisphosphate (PIP_2)-positive large vacuoles. We also support evidence that Arf6, a member of the ADP-ribosylation factor (ARF) family of GTPase (Turner and Brown, 2001), is required for vacuole formation after Gas3/PMP22 expression, but not for its accumulation within late endosomes. In conclusion we propose that increased Gas3/PMP22 expression can alter membrane traffic at different levels, and this perturbs Schwann cells myelination, thus triggering peripheral neuropathies.

Materials and Methods

Culture conditions

NIH3T3, IMR90-E1A, U2OS and primary Schwann cells were grown in Dulbecco's modified Eagle medium (DMEM) supplemented with 10% fetal calf serum (FCS), penicillin (100 U/ml), and streptomycin (100 μg/ml). Rat Schwann cells were prepared from the sciatic nerves of neonatal Wistar rats. Purified Schwann cells were grown in DMEM supplemented with 10% FCS, 2 μM forskolin and 20 μg/ml of bovine pituitary gland extract for a limited period. Transfection of U2OS cells was performed using the calcium phosphate precipitation method. The specific ROKα inhibitor Y-27632 was used at 10 μM final concentrations.

Microinjection and time lapse

Nuclear microinjection was performed using the Automated Injection System (Zeiss-Germany) as previously described (Fabbretti et al., 1995). Nuclei of the cells were injected with the different expression vectors for 0.5 seconds at the constant pressure of 50 hPa. For time-lapse analysis cells were directly plated on the petri dishes and soon after microinjection were used for the time-lapse. Time-lapse analysis was performed by using a laser scan microscopy Leica TCS NT in a 5% CO_2 atmosphere at 37°C.

Plasmid construction

For expression in eukaryotic cells human *gas3/PMP22* and its point mutated forms, L16P and N41Q (Brancolini et al., 2000) were amplified by PCR and subcloned in pEGFP-N1 vector (Clontech). The sense primer ol5′ (5′-GAGTGAATTCAACTCCGCTGAGCAG-AACTT-3′) containing an *Eco*RI site and a reverse primer ol3′ (5′-CGAGGATCCTCGCGTTTCCGCAAGATCA-3′) containing a *Bam*HI site were used.

For expression in eukaryotic cells of claudin-15 the corresponding cDNA, received from RZPD (Resource Center/Primary Database, German Human Genome Project) was amplified by PCR and subcloned in pEGFP-N1 vector (Clontech). The sense primer ol5′c (5′-CATGAATTCTGATGTCGATGGCTGTGGAAACC-3′) containing an *Eco*RI site and a reverse primer ol3′c (5′-CATGG-ATCCCGCACGTAGGCGTTTCTGCCGTA-3′) containing a *Bam*HI site were used. All constructs generated were sequenced using an automated system (ABI PRISM 310) to check for the fidelity of the inserted PCR fragments.

Immunofluorescence microscopy

For indirect immunofluorescence microscopy, cells were fixed with 3% paraformaldehyde in PBS for 20 minutes at room temperature or in methanol/acetone (1/1) at –20°C. The coverslips were treated with the different first antibodies: anti-transferrin receptor (Tnf-R) (OK-T9), anti hPLAP, anti-lysobisphosphatidic acid (LBPA), anti-VSV (Sigma), anti-FLAG (Sigma), anti-HA (Santa Cruz), anti-clathrin (Trasduction L.), anti-annexin II (Trasduction L.), anti-MHC I clone W6/32 (NeoMarkers) or with biotinylated-WGA (Boehringer), biotinylated-ConcA (Boehringer) and TRITC-phalloidin (Sigma) diluted in PBS, for 1 hour in a moist chamber at 37°C. They were then washed with PBS three times, followed by incubation with the relative secondary antibodies: TRITC-conjugated anti-mouse (Sigma), TRITC-conjugated anti-rabbit (Sigma), AlexaFluor-633-conjugated anti-rabbit (Molecular Probes), AlexaFluor-633-conjugated anti-mouse (Molecular Probes) or with TRITC-conjugated streptavidin (Molecular Probes) for 1 hour at 37°C. Cells were examined with a laser scan microscope (Leica TCS NT) equipped with a 488-534 λ Ar laser and a 633 λ He-Ne laser.

Electron microscopy

For electron microscopic (EM) examination, short term (5 days) SC cultures were established from sciatic nerves of 30-day-old homozygous PMP22 transgenic ($PMP22_{tg}$) rats, according to standard techniques. Briefly, SC were grown for 5 days in DMEM/F12 containing 10% FBS, in the presence of 10^{-5} Ara-C to eliminate contaminant fibroblasts. Cells were then rinsed, trypsinized and fixed in 2.5% glutaraldehyde in cacodylate buffer for 30 minutes. Finally, cells were post-fixed for 1 hour in 2% osmium tetroxide, dehydrated in alcohol and embedded in epoxy resin.

30-day-old $PMP22_{tg}$ rats were sacrificed and sciatic nerves quickly removed. Specimens were fixed in 2.5% glutaraldehyde in cacodylate buffer, pH 7.4, for 2 hours, post-fixed with 1% osmium tetroxide in cacodylate buffer, pH 7.4, for 1 hour, dehydrated in alcohol and embedded in epoxy resin.

Ultrathin sections, stained with 5% uranyl acetate and lead citrate, were then prepared from cultured SC and sciatic nerves, and examined under a Zeiss EM 109.

Internalization of anti-MHC I antibody and biotinylated Tfn

For MHC I antibody internalization, cells transfected with Gas3/PMP22-GFP construct were incubated with anti-MHC I antibodies for 1 hour at 37°C. To remove anti-MHC antibody remaining at the surface cells, before fixing, were washed with low pH buffer as previously described (Radhakrishna and Donaldson, 1997). In addition, cells were probed with unconjugated goat anti-mouse antibody before permeabilization for 30 minutes. Internalized MHC antibody was then visualized by probing with TRITC-conjugated goat anti-mouse in the presence of 0.2% of saponin.

For in vivo binding to biotinylated Tfn, IMR90-E1A cells were microinjected with pEGFP-N1-*Gas3/PMP22* (100 ng/μl). After 15 hours the petri dish was incubated in serum-free medium containing 20 mM HEPES pH 7.4 for 30 minutes at 37°C. Human

biotinylated transferrin (Sigma) was pre-bound to the cells on ice for 45 minutes at a concentration of 50 μg/ml. Internalization was initiated by placing the coverslips into medium containing 10% FCS and was prolonged for 2 hours at 37°C.

Western blotting and enzymatic treatments

For western blotting, proteins were transferred to 0.2 μm pore sized nitro-cellulose (S. and S.) using a semidry blotting apparatus (Pharmacia) (transfer buffer: 20% methanol, 48 mM Tris, 39 mM glycine and 0.0375% SDS). After staining with Ponceau S, the nitro-cellulose sheets were saturated for 1 hour in Blotto-Tween 20 (50 mM Tris-HCl pH 7.5, 200 mM NaCl, 5% nonfat dried milk and 0.1% Tween 20) and incubated overnight at room temperature with the anti-GFP antibody (Invitrogen). Blots were then rinsed three times with Blotto-Tween 20 and incubated with peroxidase conjugated goat anti-rabbit (Sigma) for 1 hour at room temperature. Blots were then washed four times in Blotto-Tween 20, rinsed in phosphate buffer saline and developed with Super Signal West Pico, as recommended by the manufacturer (Pierce).

PNGase-F treatment of cellular lysates and immunoblotting analysis were performed as described (Fabbretti et al., 1995). For EndoH treatment the cellular lysates were prepared in 0.5% SDS, 1% β-mercaptoethanol, denatured by 10 minutes boiling and then 50 mM sodium acetate pH 5.5, 1% NP-40 was added. After addition of 1 milliunit of Endoglycosidase H (Endo H, Boehringer), samples were incubated for 3 hours at 37°C.

Results

Characterization of the Gas3/PMP22-GFP fusion protein

To gain insight into the mechanisms triggered by Gas3/PMP22 overexpression we have produced a Gas3/PMP22-GFP fusion protein. To verify that Gas3/PMP22-GFP was normally exposed at the cell surface, U20S cells were transiently transfected with Gas3/PMP22-GFP. Cell lysates were prepared, treated with Endo-H or PNGase-F to define pre-Golgi or post-Golgi glycosylation (Brancolini et al., 2000) and subjected to western blot analysis using an anti-GFP antibody (Fig. 1A).

In untreated lysates Gas3/PMP22-GFP migrated as a diffuse band around 50 kDa and as a sharp band around 47 kDa. After PNGase-F treatment a single band migrating at around 45 kDa was observed, thus indicating that the two Gas3/PMP22 forms contain different sugar chains. The ~47 kDa band represents an immature pre-Golgi form of Gas3/PMP22-GFP, since it migrated at ~45 kDa after incubation of the lysates with Endo-H, while the ~50 kDa band represents the post-Golgi form of Gas3/PMP22.

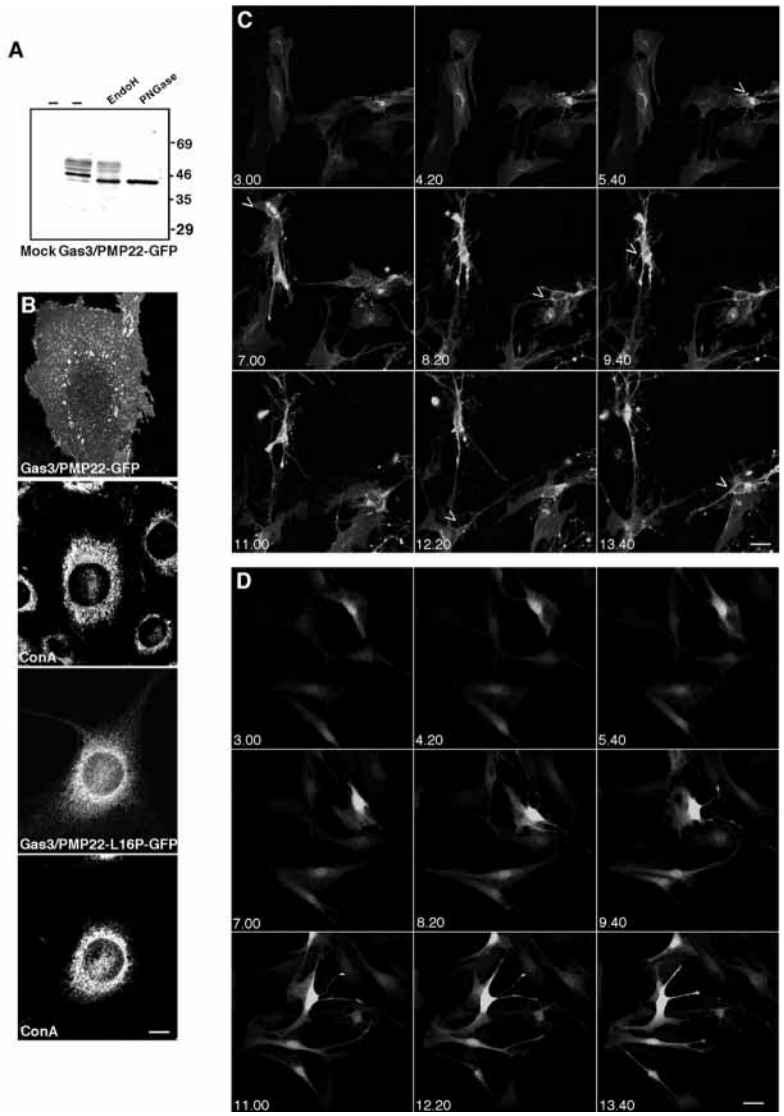

Fig. 1. Expression of the Gas3/PMP22-GFP. (A) Immunodetection of Gas3/PMP22-GFP in transfected U20S cells. U2OS cells were transfected with pEGFP-N1-*Gas3/PMP22* and cellular extracts were treated with or without PNGase-F or Endo-H as indicated. Immunodetection was performed using the anti-GFP antibody. (B) Subcellular localization of Gas3/PMP22-GFP and Gas3/PMP22-L16P-GFP. *Gas3/PMP22-GFP* and *Gas3/PMP22-L16P-GFP* were overexpressed in NIH3T3 by nuclear microinjection. 6 hours after microinjection, cells were fixed and double-stained to visualize GFP and ER, using biotinylated concanavalin A. Bar, 18 μm. (C) Time-lapse images of Schwann cells overexpressing Gas3/PMP22-GFP. Frames at selected hours after microinjection, as indicated, showing Schwann cells overexpressing Gas3/PMP22-GFP. Arrowheads underline a reduction in spreading; asterisks indicate floating dead cells. (D)Time-lapse images of Schwann cells overexpressing GFP. Frames at selected hours after microinjection showing Schwann cells overexpressing GFP. Bar, 30 μm.

To confirm that Gas3/PMP22-GFP was normally exposed at the cell surface, pEGFP-N1-*Gas3/PMP22* was microinjected in the nucleus of NIH3T3 cells and 6 hours later the cells were fixed and analyzed to define Gas3/PMP22-GFP subcellular distribution. Double immnuofluorescence analysis using biotinylated concanavalin A, a lectin that is specific for mannose residues, which are enriched in the endoplasmic reticulum (ER) compartment, showed that Gas3/PMP22-GFP was uniformly distributed at the cell surface and it was not retained in the ER (Fig. 1B). By contrast, the point mutated derivative Gas3/PMP22-L16P-GFP, used as control, accumulated in the perinuclear area, largely overlapping the

concanavalin A staining (Fig. 1B) as previously reported (Brancolini et al., 2000).

We next performed a time-lapse analysis to evaluate the ability of Gas3/PMP22-GFP to regulate cell spreading and death (Brancolini et al., 1999). The time-lapse analysis was performed in primary Schwann cells and frames were collected every 3 minutes during the period of 24 hours. Selected frames of a representative experiment, at the indicated hours, are shown in Fig. 1C. As a control we overexpressed GFP alone and the time-lapse analysis is shown in Fig. 1D. Gas3/PMP22-GFP triggers changes in cell spreading (arrowheads, Fig. 1C) and cell death, (see cell shrinkage and fragmentation, asterisks Fig. 1C); while GFP alone was unable to induce such changes. Similar results have been obtained in NIH3T3 and U2OS cell lines (data not shown).

Together these results indicate that addition of the GFP to Gas3/PMP22 does not interfere with its post-translational maturation, its subcellular localization and its ability to modulate cell shape.

Accumulation of vacuoles in cells expressing Gas3/PMP22

A more detailed analysis of the time-lapse shown in Fig. 1C demonstrated that Gas3/PMP22 causes accumulation of vacuoles before the appearance of overt changes in cell shape. In Schwann cells Gas3/PMP22-GFP can be initially visualized as a diffuse staining at the cell surface and as small vesicles, clustered in the perinuclear region (see arrowhead time-frame 3.00, Fig. 2A). Later, vacuoles showing intense staining for Gas3/PMP22-GFP can be observed in limited areas of the cells (see asterisks at time-frames 5.40, 6.40, 7.04). The appearance of these vacuoles anticipated changes in cell morphology. The time-lapse studies were next performed in NIH-3T3 cells. As shown in Fig. 2B, here again Gas3/PMP22 can be visualized as a diffuse staining and as small vesicles clustered in the perinuclear region (see arrowhead time-frame 3.03, Fig. 2B). At later stages, accumulation of vacuoles that increased in number and size were observed (arrows, Fig. 2B). From the data presented in Fig. 2B it appears clearly that the retraction from adhesion substrate occurs only at later times with respect to vacuole accumulation and can be confirmed by the rapid movement of the peripheral vacuoles marked by the asterisk (Fig. 2B).

Finally we analyzed whether vacuoles could be identified in SC from homozygous PMP22 transgenic rats (Sereda et al., 1996). Electron microscopy analysis of sciatic nerves obtained at 30 days of age provide evidence that SC contained intracellular myelin figures, which are not associated with the axon (Fig. 2C, arrow) and vacuoles (Fig. 2C, asterisks), as previously observed (Niemann et al., 2000). Similar structures were never observed in control sciatic nerves (data not shown). Interestingly, electron microscopic analysis of cultured SCs obtained from homozygous rats showed strikingly similar intracytoplasmic periodic structures (Fig. 2D, arrow) entrapping vacuoles. Although we cannot exclude that they are myelin debris or products of abnormal myelin assembly, we never observed similar inclusions in control cultured SC (data not shown).

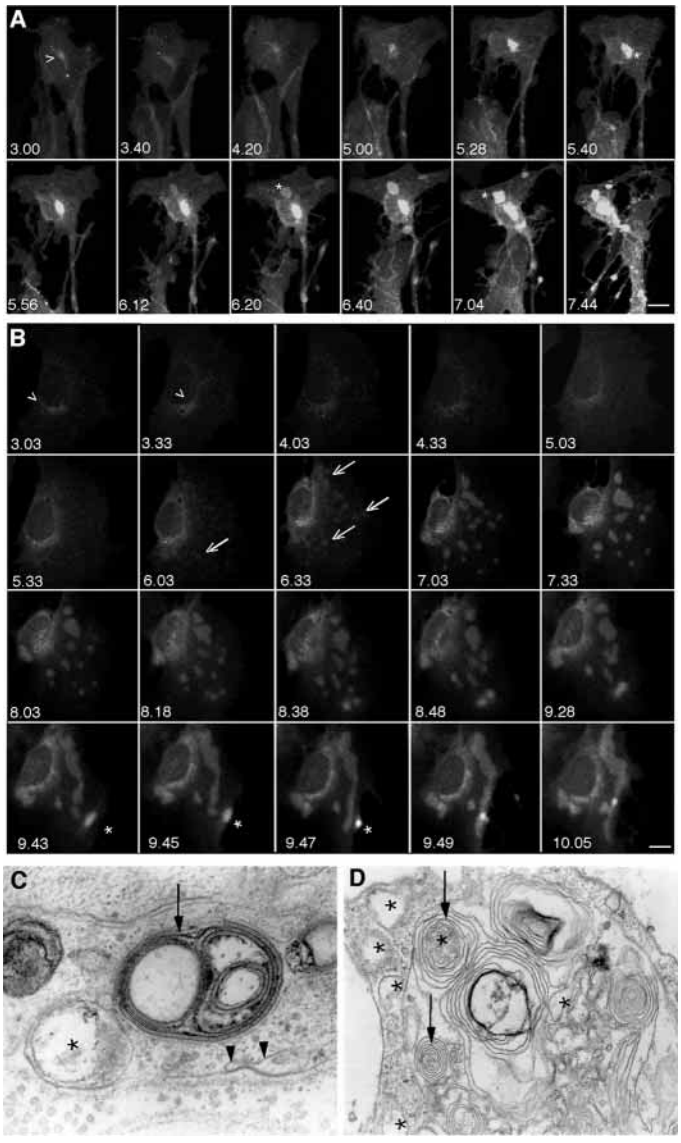

Fig. 2. Accumulation of membrane vesicles in cells expressing Gas3/PMP22. (A) Time-lapse images of SCs overexpressing Gas3/PMP22-GFP. Frames at selected hours after microinjection, as indicated, showing Schwann cells overexpressing Gas3/PMP22-GFP. Arrowhead indicates cluster of vesicles in the perinuclear region and asterisks indicate vacuoles. Bar, 18 μm. (B) Time-lapse images of NIH-3T3 cells overexpressing Gas3/PMP22-GFP. Frames at selected hours after microinjection, as indicated, of a representative cell injected with pEGFP-N1-*Gas3/PMP22* (10 ng/μl) are shown. Arrowhead indicates cluster of vesicles in the perinuclear region; arrows indicate vacuoles; asterisks indicate a vacuole close to the area retracted from the adhesion substrate. Bar, 14 μm. (C) Electron micrograph of a SC from sciatic nerve of homozygous $PMP22_{tg}$ rat, 100,000×. Intracellular myelin figures not associated with an axon are present (arrow). Moreover, empty vacuoles made up by redundant layers of SC membrane (asterisk) and plasma membrane invagination (arrowhead) can be observed. (D) Electron micrograph of a homozygous $PMP22_{tg}$ SC in culture (5 days), 60,000×. Concentric sheaths of membrane are present in the cytoplasm (arrows). Vacuoles can be observed either in the centre of the layer, or related to the SC membrane (asterisk).

Gas3/PMP22-dependent accumulation of vacuoles was independent of Rho-Kinase and Bcl-2

Studies in cultured cells have demonstrated that Gas3/PMP22 can regulate cell spreading and cell death. The effect on cell spreading was dependent on the small GTPase RhoA, while the proto-oncogene Bcl-2 counteracted the apoptotic response (Brancolini et al., 1999). Therefore we decided to investigate whether the accumulation of vacuoles induced by Gas3/PMP22 could be suppressed by co-expression of Bcl-2 or by a constitutively active form of RhoA. To further characterize the Rho pathway suppressing the effect of Gas3/PMP22 on cell adhesion, we decided to use the Rho-kinase, an important downstream effector of RhoA that regulates cell contractility and morphology (Leung et al., 1996; Matsui et al., 1996; Ishizaki et al., 1997). We first observed that co-expression of a constitutively active form of Rho-Kinase (ROKα1-1271), but not the kinase-dead mutant ROKαK112A, suppressed the effect of Gas3/PMP22 on cell spreading in NIH3T3 fibroblasts (Fig. 3A). Representative fields of cells co-expressing Gas3/PMP22-GFP and ROKα1-1271, or Gas3/PMP22-GFP and ROKαK112A are shown in Fig. 3B.

REF 52 cells are weakly responsive to Gas3/PMP22 overexpression (Brancolini et al., 1999), thus representing a suitable system to analyze whether endogenous ROKα activity is required to counteract the Gas3/PMP22 effect. Cells were microinjected with Gas3/PMP22-GFP and 21 hours later incubated with Y-27632 (10 μM), a specific inhibitor of Rho kinase (Uehata et al., 1997), for 1 hour. As shown in Fig. 3A, the addition of Y-27632 resulted in dramatic changes of cell shape in cells overexpressing Gas3/PMP22. By contrast, overexpression of Gas3/PMP22 in the absence of the inhibitor was insufficient to consistently alter cell shape. Representative fields of cells expressing Gas3/PMP22-GFP, hPLAP alone, or in the presence of Y-27632 are shown in Fig. 3D. These results suggest that Rho kinase can suppress the effect induced by Gas3/PMP22 on cell spreading.

Next, we analyzed whether the constitutively active form of Rho-Kinase (ROKα1-1271), or Bcl-2 were able to interfere with the accumulation of vacuoles induced by Gas3/PMP22 overexpression. hPLAP and the kinase-dead mutant ROKαK112A were co-expressed as controls. Cells co-expressing Gas3/PMP22-GFP and the different tested genes were scored for accumulation of vacuoles, by immunofluorescence analysis.

When hPLAP or ROKαK112A were co-expressed, Gas3/PMP22 induced accumulation of vacuoles in ~30% of the cells (30.2±8.4 and 32.4±4.9, respectively) as shown in Fig. 3E. Co-expression of the constitutively active Rho-kinase or of Bcl-2 did not suppress the accumulation of vacuoles, but instead we observed an increase in the percentage of cells presenting vacuoles (45.1±2.4 and 42.9±3.7).

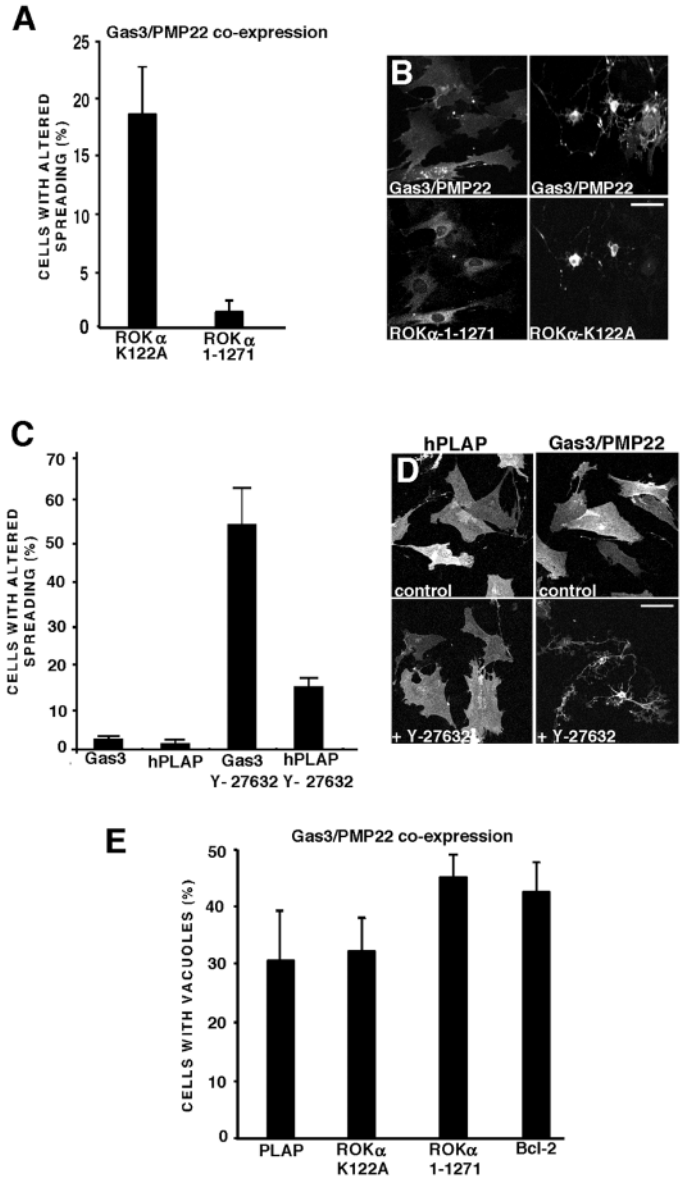

Fig. 3. ROKα and Bcl-2 are unable to suppress vacuoles accumulation in cells expressing Gas3/PMP22. (A) The indicated ROKα constructs were co-expressed with *gas3/PMP22-GFP* in NIH3T3 cells. After 24 hours from microinjection cells were fixed and processed for immunofluorescence to detect Gas3/PMP22-GFP and ROKα as described in Materials and Methods. Cells were scored for reduced spreading as previously described (Brancolini et al., 1999). Data represent arithmetic means±s.d. for four independent experiments. (B) Immunofluorescence analysis of NIH3T3 cells co-expressing gas3/PMP22-GFP and ROKα1–1271 or Gas3/PMP22-GFP and ROKα K112A. NIH3T3 cells 24 hours after seeding were microinjected with pEGFP-N1-*gas3/PMP22* (20 ng/μl) and pXJ40-ROKα1–1271 (80 ng/μl) or with pXJ40- ROKα K112A (80 ng/μl). After 24 hours cells were fixed and processed for immunofluorescence to visualize Gas3/PMP22 and HA-tagged ROKα. Bar, 18 μm. (C) Gas3/PMP22-GFP and hPLAP, as controls, were overexpressed in REF 52 cells. After 21 hours from microinjection 10 μM of Y-27632 (final concentration) was added to the culture medium and cells were fixed 1 hour later and processed for immunofluorescence to score the Gas3/PMP22 phenotype. Data represent arithmetic means±s.d. for four independent experiments. (D) Immunofluorescence analysis of REF 52 cells expressing Gas3/PMP22-GFP or hPLAP treated or not with Y-27632. REF 52 cells 24 hours after seeding were microinjected with pEGFP-N1-*gas3/PMP22* (20 ng/μl) or with pGDSV7S-*hPLAP* (80 ng/μl). Bar, 18 μm. (E) Gas3/PMP22-GFP and the indicated genes were co-expressed in NIH3T3 cells. After 18 hours from microinjection cells were fixed and processed for immunofluorescence to visualize Gas3/PMP22-GFP and the co-expressed protein. Cells were scored for accumulation of vacuoles. Data represent arithmetic means±s.d. for four independent experiments.

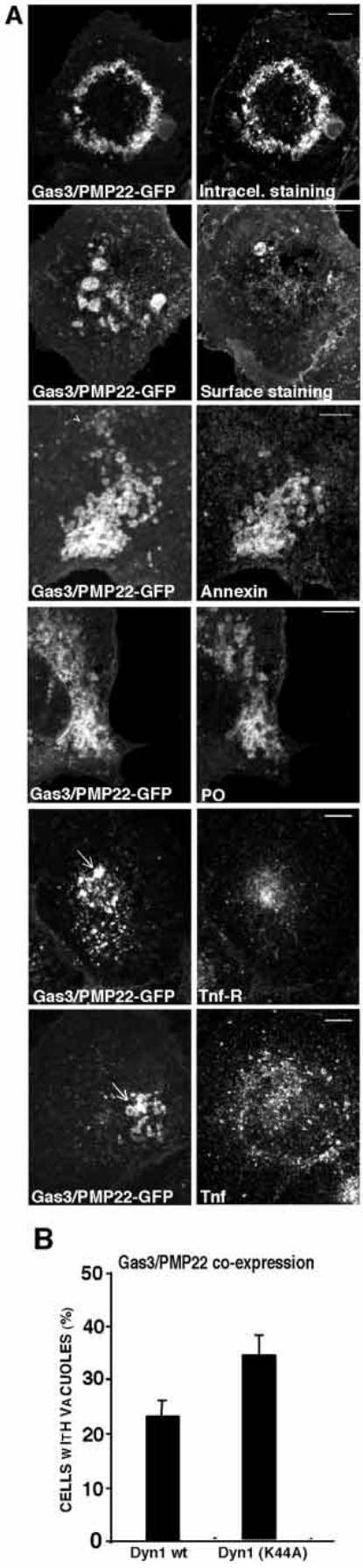

Fig. 4. Characterization of the Gas3/PMP22-positive vacuoles. (A) NIH3T3 or IMR90-E1A cells were microinjected with Gas3/PMP22-GFP and 12 hours later were fixed and probed with antibodies to annexin II, Tfn-R, and P0 or stained with WGA as indicated. Endocytosis of biotinylated Tfn was performed as described in Materials and Methods. The arrowhead indicates vacuoles negative for annexin II staining, whereas arrows point to vacuoles negative for Tfn-R and Tfn staining. Bar, 8 μm. (B) Dynamin1 wt and the point mutated derivative K44A defective in GTP binding and hydrolysis were co-expressed with Gas3/PMP22-GFP. After 18 hours from microinjection cells were fixed and processed for immunofluorescence to detect Gas3/PMP22-GFP and dynamin as described in Materials and Methods. Cells were scored for accumulation of vacuoles. Data represent arithmetic means±s.d. for four independent experiments.

Characterization of the Gas3/PMP22-positive vacuoles

We next decided to characterize the vacuoles induced by Gas3/PMP22 expression in more detail. We noticed that these vacuoles were inside the cells as their labeling with biotinylated lectin WGA was possible only after permeabilization (Fig. 4). We observed that annexin II, a peripheral membrane protein (Merrifield et al., 2001), is enriched in the Gas3/PMP22-GFP labeled vacuoles. Interestingly, clusters of small vacuoles positive for Gas3/PMP22-GFP do not contain annexin II (see arrowhead, Fig. 4). Also, integral membrane proteins such as P0 (D'Urso et al., 1990) and N-cadherin (data non-shown) when co-expressed accumulated in these vacuolar membranes (Fig. 4). Here again not all the Gas3/PMP22-positive vacuoles were marked for P0. Neither γ-adaptin, a component of the AP-1 complex (Hirst and Robinson, 1998) and marker of the TGN, nor clathrin labeled the Gas3/PMP22-positive vacuoles (data not shown). To exclude that the Gas3/PMP22 vacuoles were ER proliferations, cells were stained with an anti-calreticulin antibody as a marker of ER. Intracellular vacuoles labelled with Gas3/PMP22-GFP were negative for calreticulin (data not shown).

The localization of Gas3/PMP22 in clusters of small vesicles in the perinuclear region (Fig. 1) is reminiscent of recycling vesicles (Yamashiro et al., 1984; Daro et al., 1996; Ren et al., 1998). These recycling vesicles contain cargo that will be recycled back to the cell surface (Daro et al., 1996) such as transferrin (Tnf) bound to its receptor (Tfn-R). We next examined the distribution of Tfn and Tfn-R in IMR90-E1A human fibroblasts expressing Gas3/PMP22-GFP by immunofluorescence analysis. As exemplified in Fig. 4A, vacuoles containing Gas3/PMP22-GFP were negative for Tfn-R. We confirmed these data after the endocytosis of biotinylated Tfn prebound in the cold to plasma membrane (PM) Tfn receptor. After growing for 3 hours in serum-free medium, cells were fixed and processed for the analysis. As shown in Fig. 4A, vacuoles containing Gas3/PMP22 were negative for Tfn.

A role for dynamin in clathrin-mediated endocytosis is well established (Hinshaw, 2000). Overexpression of a dominant negative mutant of dynamin-1 (dyn1; K44A) potently inhibited receptor-mediated endocytosis of Tfn, but other membrane trafficking events including fluid-phase endocytosis are unaffected (Altschuler et al., 1998). To confirm that the accumulation of vacuoles in response to Gas3/PMP22 expression was unrelated to the receptor-mediated endocytosis,

we investigated the effect of dyn1 (K44A) on vacuole appearance. Co-expression of dyn1 wt was used as a control. Fig. 4B shows that co-expression of dyn1 (K44A) has no effect on the accumulation of vacuoles in response to Gas3/PMP22. In contrast, we observed an increase in the number of cells expressing Gas3/PMP22-GFP and accumulating vacuoles when dyn1 (K44A) was co-expressed instead of dyn wt. Under the same experimental conditions dyn1 (K44A) inhibited receptor-mediated endocytosis (data not shown).

Gas3/PMP22-vacuoles are positive for Arf6 and Arf6 Q67L

A plasma membrane recycling pathway that, in some cell types is distinct from transferrin-positive endosome has been recently characterized. The ADP-ribosylation factor 6 (Arf6) regulates the movement of membrane between the plasma membrane and this nonclathrin-derived endosomal compartment (Radhakrishna and Donaldson, 1997). Arf6 localizes to the PM in its GTP state and to an internal juxtanuclear compartment that exhibits tubular elements in its GDP-bound state (Peters et al., 1995; Radhakrishna and Donaldson, 1997). Arf6 mutants Q67L and T27N are predicted to be in the GTP- or the GDP-bound states respectively (Peters et al., 1995; Radhakrishna and Donaldson, 1997). Therefore, to understand the relationships between this nonclathrin-derived endosomal compartment and Gas3/PMP22, we first compared the subcellular distribution of Gas3/PMP22 and Arf6. NIH3T3 cells co-expressing Gas3/PMP22 and Arf6, Arf6-Q67L or Arf6-T27N were analyzed by confocal microscopy.

The vacuolar membrane induced by Gas3/PMP22 were also positive for Arf6 and Arf6 Q67L (Fig. 5). In addition we observed that when Gas3/PMP22 and Arf6-Q67L were overexpressed, vacuoles were more often present in compact clusters. The co-localization of Gas3/PMP22 with Arf6-T27N, which accumulates in the endocytic tubular compartment, was less evident (Fig. 5). Sporadically vesicular structures were double-positive for Arf6 T27N and Gas3/PMP22 (Fig. 5, arrowhead), moreover Gas3/PMP22-positive vacuoles were rarely observed (see below).

p95-APP1, a member of the GIT family of ARF-GAP and a putative GAP for Arf6 has been recently identified (Di Cesare et al., 2000). Overexpression of a truncated form of p95-APP1, that lacks the ARF-GAP domain, triggers the accumulation of large vesicles that co-localize with Arf6T27N and markers of the endocytic pathway, including transferrin receptor and Rab11 (Matafora et al., 2001). To further confirm that Gas3/PMP22 vacuoles do not co-localize with the endocytic compartment containing the GDP-bound form of Arf6 we co-expressed Gas3/PMP22 and p95-APP1 deleted in its ARF-GAP domain (p95-C3) to evaluate whether they can induce different types of vacuoles. As exemplified in Fig. 5, two different types of vacuoles can be identified in cells co-expressing Gas3/PMP22 and p95-C3.

Vacuoles induced by Gas3/PMP22 are positive for PIP_2 and co-localize with internalized MHC I

Expression of Arf6 GTP hydrolysis-resistant mutant (Q67L) induces the formation of PIP_2-positive vacuoles, through the activation of PIP5-kinase (Brown et al., 2001). To confirm the relationships between Gas3/PMP22 and Arf6 we investigated whether vacuoles induced by Gas3/PMP22 were also enriched in PIP_2. PIP_2 was visualized by co-expressing a plasmid encoding the pleckstrin homology domain of PLC-δ tagged with GFP (PH-GFP), which has previously been characterized as a marker of PIP_2 distribution in the cells (Varnai and Balla, 1998).

We assessed the distribution of PIP_2 in U2OS (Fig. 6A) and NIH3T3 cells (Fig. 6B) co-expressing Gas3/PMP22-VSV and PH-GFP. Overall Gas3/PMP22 and PH-GFP exhibited a remarkable co-localization at the cell surface and we found that the large vacuoles labeled for Gas3/PMP22-VSV were also positive for PH-GFP. As a control we assessed the distribution of PIP_2 in NIH3T3 and U2OS cells expressing the point-mutated derivatives of Gas3/PMP22 (L16P) responsible for the CMT1A. This mutant does not reach the PM, accumulates in

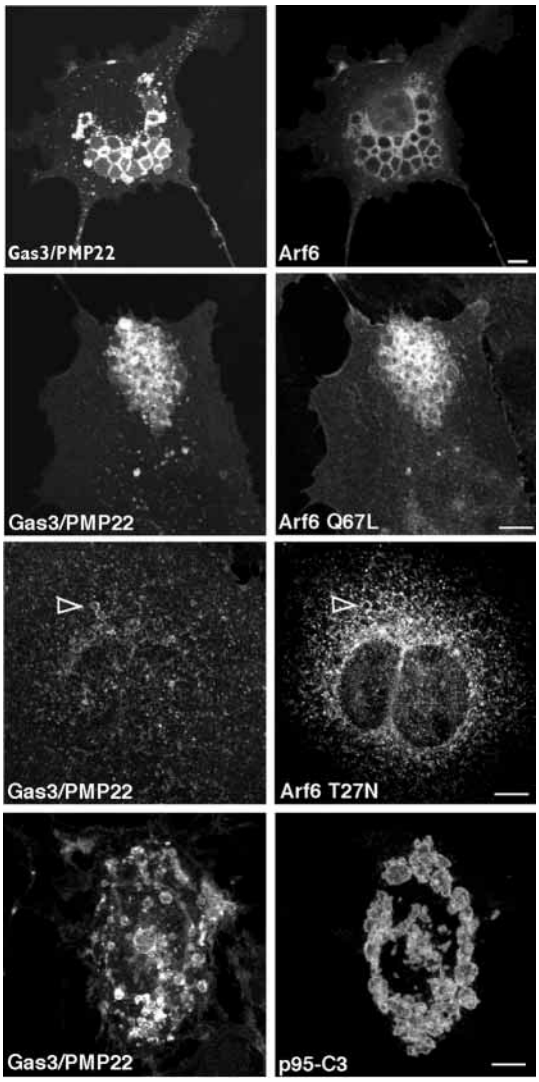

Fig. 5. Gas3/PMP22 co-localizes with Arf6 and Arf6-Q67L in vacuoles. NIH3T3 cells were co-injected with Gas3/PMP22-GFP and with HA-tagged Arf6, Arf6-Q67L, Arf6-T27N or FLAG-tagged p95-C3. 18 hours later cells were fixed and probed with antibody to HA to visualize Arf6 and the different mutants or with antibody to FLAG to visualize p95-C3 as shown. Bar, 8 μm.

ER and eventually forms aggresomes (Brancolini et al., 2000; Naef and Suter, 1999; Notterpek et al., 1999). The above described vacuoles were undetectable when Gas3/PMP22-L16P was expressed; moreover, PH-GFP did not co-localize with Gas3/PMP22-L16P. By contrast, a glycosylation deficient mutant Gas3/PMP22-MG (Brancolini et al., 2000) was able to trigger accumulation of vacuoles that were PIP_2 positive (Fig. 6B).

To further characterize the vacuoles induced by Gas3/PMP22 cells were labeled with antibody against MHC I, a marker for the Arf6 endosomal pathway (Radhakrishna and Donaldson, 1997). As shown in Fig. 6C, MHC I accumulated in a large part of the Gas3/PMP22-positive vacuoles. In addition we used antibody internalization over 60 minutes to determine whether surface MHC I can enter the cells and accumulate in the same vacuoles that accumulate Gas3/PMP22. In both IMR90-E1A and U2OS cells expressing Gas3/PMP22, MHC I antibody was found in vacuoles also accumulating Gas3/PMP22 (Fig. 6D-E). However, it should be noted that not all the vacuoles containing Gas3/PMP22 were loaded with MHC I. It is possible that these vacuoles, negative for MHC I, represent internal membrane that has been accumulated before the addition of the MHC I antibody.

Vacuoles containing Gas3/PMP22 that are not coated with actin are positive for LBPA, a late endosome marker

We also analyzed whether vacuoles induced by Gas3/PMP22 were coated with actin as previously described for vacuoles induced by Arf6-Q67L (Brown et al., 2001). Fig. 7 shows that vacuoles induced by Arf6-Q67L were coated with actin and present in large clusters as expected. Interestingly, vacuoles induced by Gas3/PMP22 were also coated with actin. However some differences were observed: in the case of Gas3/PMP22, some vacuoles, generally not clustered at the periphery of the cells, did not present a coat of actin (see arrowheads, Fig. 7). These vacuoles not coated with actin were also negative for PIP_2 (see inset, Fig. 7).

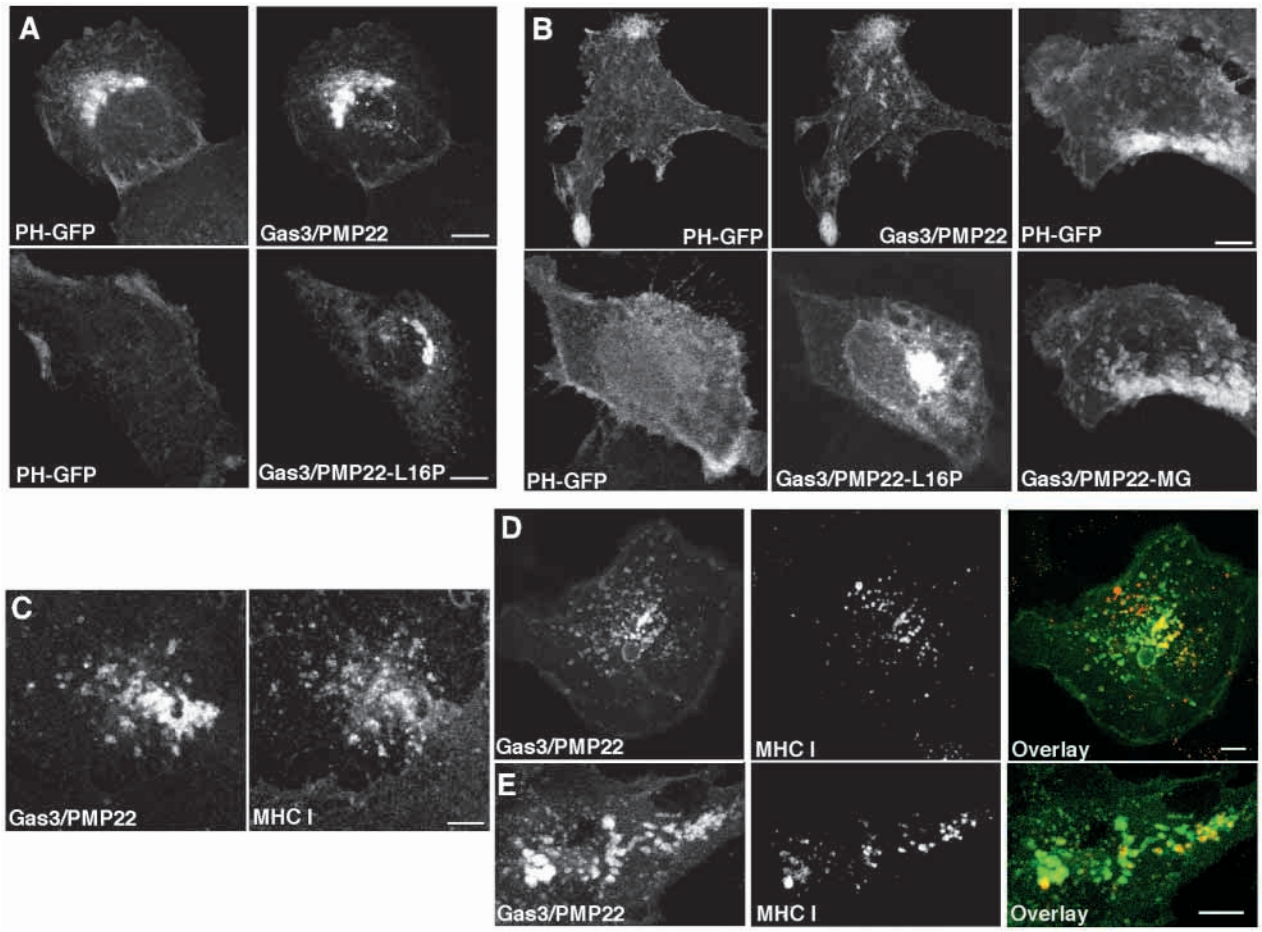

Fig. 6. Gas3/PMP22-induced vacuoles are PIP_2-positive and trap MHC I. (A) U2OS cells were transfected with Gas3/PMP22-VSV and PH-GFP or with Gas3/PMP22-L16P-VSV and PH-GFP. 40 hours later cells were fixed and probed with an antibody to VSV. Bar, 8 μm. (B) NIH3T3 cells were co-injected with Gas3/PMP22-VSV and PH-GFP, with Gas3/PMP22-L16P-VSV and PH-GFP or with Gas3/PMP22-MG-VSV and PH-GFP. 18 hours later cells were fixed and probed with antibody to VSV to visualize Gas3/PMP22. Bar, 8 μm. (C) IMR90-E1A cells were microinjected with Gas3/PMP22-GFP. 15 hours later cells were fixed and probed with an antibody to MHC I. Bar, 4 μm. (D) IMR90-E1A cells were microinjected with Gas3/PMP22-GFP. 15 hours later they were allowed to internalize MHC I antibody for 60 minutes and then were fixed and processed for visualizing internalized antibody. Bar, 5 μm. (E) U2OS cells were microinjected with Gas3/PMP22-GFP. 18 hours later they were allowed to internalize MHC I antibody for 60 minutes and then were fixed and processed for visualizing internalized antibody. Bar, 5 μm.

To characterize vacuoles positive to Gas3/PMP22, but negative for PIP_2 and actin, cells were labelled with an antibody specific for lysobisphosphatidic acid (LBPA), a marker of late endosomes (Kobayashi et al., 1998). As shown in Fig. 8A (arrowheads), some Gas3/PMP22-positive vacuoles, located in the perinuclear region, were also marked with LBPA. Other Gas3/PMP22-positive vacuoles, generally more peripheral and larger, do no overlap with LBPA (as clearly shown in Fig. 8B, arrow). It is interesting to note that uninjected cells exhibited the characteristic distribution of late endosomes, which were more concentrated in the perinuclear area, but also extended towards the cell periphery. In contrast, cells that accumulated Gas3/PMP22 in the late endosomes presented a striking aggregation of them in few clusters close to the perinuclear region of the cells (Fig. 8C, arrowheads).

Gas3/PMP22 shares significant sequence identity and structural similarity with claudin, a family of more than 20 proteins that have a role in tight-junction formation and in the establishment of the ionic selectivity of the junctional barrier (Tsukita et al., 2001). Among them claudin-15 shows the higher similarity to Gas3/PMP22. Therefore we decided to study whether claudin-15 overexpression could trigger vacuole accumulation, as in the case of Gas3/PMP22. As shown in Fig. 8D, overexpressed claudin-15-GFP accumulated in vesicles, which largely overlapped with the late endosomes. However, differentially from Gas3/PMP22, claudin-15 could not trigger the accumulation of large vacuoles positive for annexin II (Fig. 8E,F, arrowhead), or Arf6 (data not shown). Interestingly, claudin-15 was also unable to trigger changes in cell shape and spreading when compared with Gas3/PMP22 (data not shown).

Finally, to confirm that Gas3/PMP22 accumulates into different types of vacuole we performed a triple co-localization to visualize Gas3/PMP22-GFP, actin and LBPA. As shown in Fig. 8G, vacuoles containing Gas3/PMP22 and coated with actin (arrows) were negative for LBPA. By contrast, vesicles containing Gas3/PMP22 and positive for LBPA were not coated with actin.

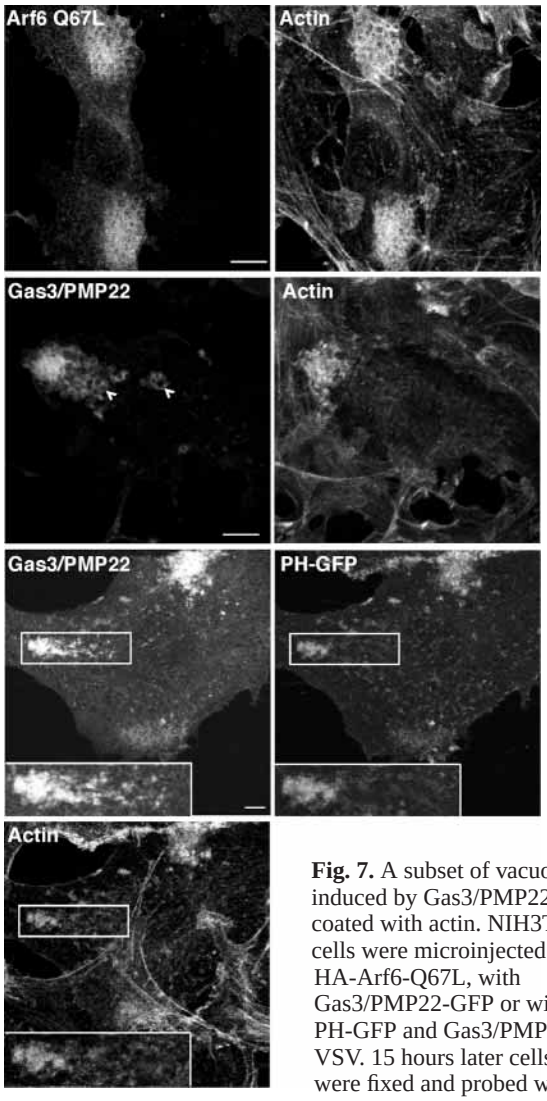

Fig. 7. A subset of vacuoles induced by Gas3/PMP22 are coated with actin. NIH3T3 cells were microinjected with HA-Arf6-Q67L, with Gas3/PMP22-GFP or with PH-GFP and Gas3/PMP22-VSV. 15 hours later cells were fixed and probed with an antibody to HA and phalloidin (top), with phalloidin (middle), or with an antibody to VSV and phalloidin (bottom) as shown. (Inset) Enlargement of box showing differences in actin coating and PIP_2 accumulation in Gas3/PMP22 vacuoles. Bar, 3 μm.

Gas3/PMP22 requires Arf6 to induce vacuoles but its accumulation in the late endosomes is independent from Arf6

To further assess the relationship between Arf6 and Gas3/PMP22 we analyzed whether Arf6-T27N, the dominant negative Arf6 mutant defective in GTP binding, could interfere with the induction of PIP_2 and Arf6-positive vacuoles in cells overexpressing Gas3/PMP22. To prevent late endosomes where Gas3/PMP22 aggregates from being counted as Arf6 endosomal vacuoles, only large vacuoles double positive for Arf6 and Gas3/PMP22 were considered for this analysis.

In NIH3T3 cells, Gas3/PMP22-GFP and Arf6, Arf6-Q67L or Arf6-T27N were co-expressed by nuclear microinjection of the respective cDNAs. We co-expressed, as a control, PH-GFP with Arf6, Arf6-Q67L and Arf6-T27N. Eighteen hours after microinjection cells were fixed and processed for immunofluorescence.

Co-expression of Arf6-T27N with Gas3/PMP22 induced a dramatic reduction in the percentage of cells presenting Gas3/PMP22-positive vacuoles (Fig. 9A). Vacuoles were formed when Gas3/PMP22 and Arf6 were co-expressed, but were not formed when Arf6 and PH-GFP were co-expressed, as previously indicated (Fig. 9A,B).

Having demonstrated that the formation of vacuoles after Gas3/PMP22 overexpression was dependent on Arf6, we next wanted to investigate whether Arf6 was required for the accumulation of Gas3/PMP22 within the late endosomes. It is possible that Gas3/PMP22 could move from the Arf6 endosomal compartment and accumulate within the late endosomes and therefore Arf6-T27N could suppress this traffic.

To this end, Gas3/PMP22-GFP and Arf6, or Arf6-T27N were co-expressed by nuclear microinjection of the respective cDNAs in NIH3T3 cells. Eighteen hours after microinjection cells were fixed and processed for immunofluorescence to visualize LBPA and Gas3/PMP22. Only vacuoles double positive for LBPA and Gas3/PMP22 were scored for this analysis.

Arf6-T27N failed to prevent the accumulation of Gas3/PMP22 in the late endosomes (Fig. 9C). Under the same experimental conditions Arf6-T27N reduced the percentage of

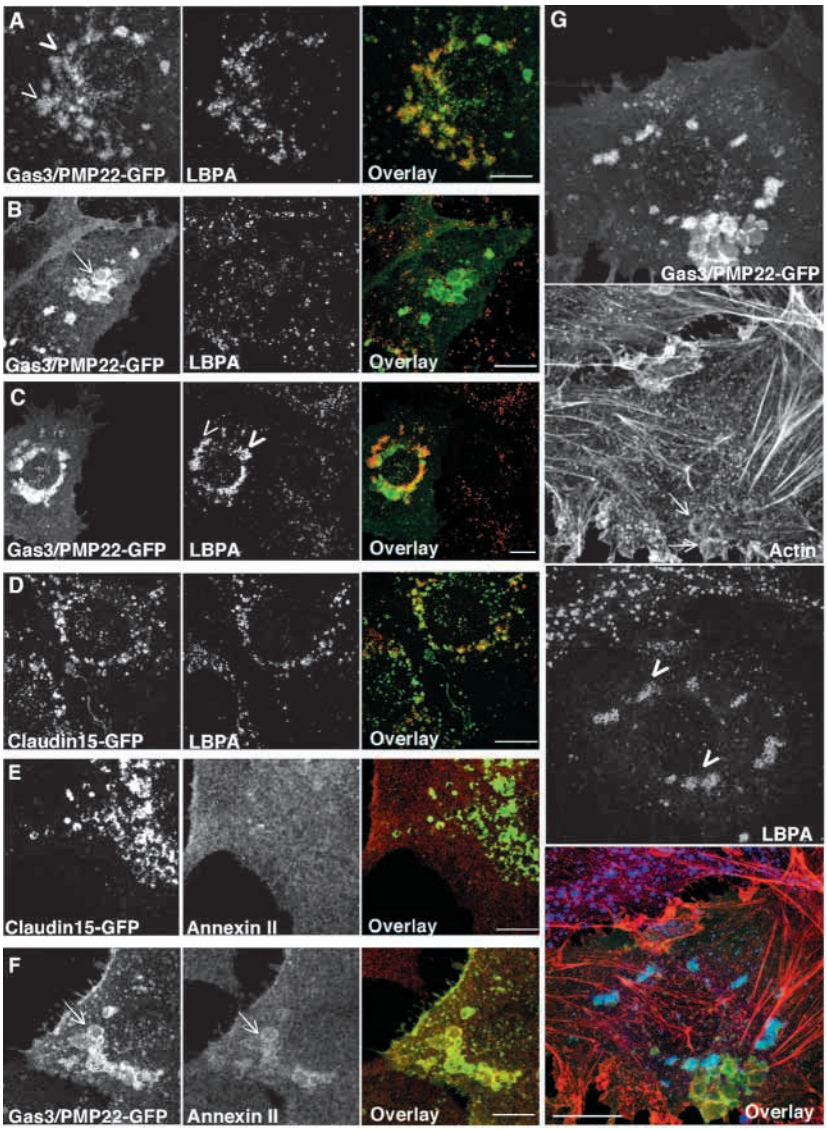

Fig. 8. Overexpressed Gas3/PMP22 was route to the late endosomes. (A) NIH3T3 cells were microinjected with Gas3/PMP22-GFP. 15 hours later cells were fixed and probed with an antibody to LBPA. Arrowheads indicate vacuoles in the perinuclear region double positive for Gas3/PMP22 and LBPA. (B) NIH3T3 cells were microinjected with Gas3/PMP22-GFP. 15 hours later cells were fixed and probed with an antibody to LBPA. The arrow indicates large peripheral vacuoles negative for LBPA staining. (C) NIH3T3 cells were microinjected with Gas3/PMP22-GFP. 15 hours later cells were fixed and probed with an antibody to LBPA. Arrowheads indicate clusters of aggregated vacuoles in the perinuclear region double positive for Gas3/PMP22 and LBPA. (D) NIH3T3 cells were microinjected with Claudin-15-GFP. 15 hours later cells were fixed and probed with an antibody to LBPA. (E) NIH3T3 cells were microinjected with Claudin-15-GFP. 15 hours later cells were fixed and probed with an antibody to annexin II. (F) NIH3T3 cells were microinjected with Gas3/PMP22-GFP. 15 hours later cells were fixed and probed with an antibody to annexin II. Arrows indicate large peripheral vacuoles positive for annexin II staining. (G) NIH3T3 cells were microinjected with Gas3/PMP22-GFP. 15 hours later cells were fixed and probed with an antibody to LBPA and phalloidin TRITC. Arrows indicate large peripheral vacuoles coated with actin and arrowheads point to clusters of aggregated vacuoles in the perinuclear region double positive for Gas3/PMP22 and LBPA. Images were obtained using a Leica TCS confocal microscopy and in the overlay are displayed in pseudocolors: green (GFP fused proteins), red (LBPA, annexin II and actin) blue (LBPA). Bar, 5 μm.

cells accumulating large vacuoles positive for Gas3/PMP22, but negative for LBPA, as demonstrated above (data not shown).

Discussion

Gas3/PMP22 plays a critical role in the majority of inheritable demyelinating peripheral neuropathies. Since duplication of the *gas3/PMP22* locus is the most common genetic alteration responsible for the CMT1A disease, a number of different studies have addressed the effect of increasing gas3/PMP22 dosage in various animal models and cellular systems. Gas3/PMP22 can regulate cell growth, apoptosis and cell adhesion when overexpressed in cultured cells (Fabbretti et al., 1995; Zoidl et al., 1997; Brancolini et al., 1999; Notterpek et al., 2001). However, the molecular link between the function of Gas3/PMP22 observed in vitro and myelin stability is still a mystery. In this manuscript we have shown that increasing Gas3/PMP22 dosage can result in the trapping of membranes in PIP_2-positive vacuolar structures. These vacuoles, which accumulate integral and peripheral membrane proteins, become enlarged probably due to the fusion of smaller vacuoles (Fig. 2B). Transferrin receptor and transferrin were absent from these vacuoles, thus suggesting that Gas3/PMP22-induced vacuoles represent membrane compartments that are distinct from transferrin-positive endosomes.

It is well established that plasma membrane dynamics in response to environmental changes are regulated by rearrangements of actin cytoskeleton (Hall, 1998; Sechi and Wehland, 2000). Recently, different studies have suggested that membrane traffic can contribute to regulate PM architecture, through the insertion and uptake of membrane at the PM (Bajno et al., 2000; Mellman, 2000; Palacios et al., 2001; Ridley, 2001). Arf6, a member of the ADP-ribosylation factor (ARF) family of GTPases is an important regulator of the PM architecture. The Arf6 GTPase cycle regulates the movement of membranes between the PM and an endosomal compartment. When in the GTP state Arf6 localizes at the PM and stimulates actin rearrangements, when in the GDP state it localizes at the endosomal compartment (Peters et al., 1995; Radhakrishna and Donaldson, 1997). Expression of the Arf6 GTP hydrolysis-resistant mutant Q67L triggers the accumulation of vacuoles, which, although more frequently clustered, resemble those induced by Gas3/PMP22 (Brown et al., 2001). Similarly to Gas3/PMP22, Arf6 vacuoles trap integral and peripheral proteins, but not Tfn-R (Brown et al., 2001). When Arf6-Q67L or Arf6 were co-expressed with

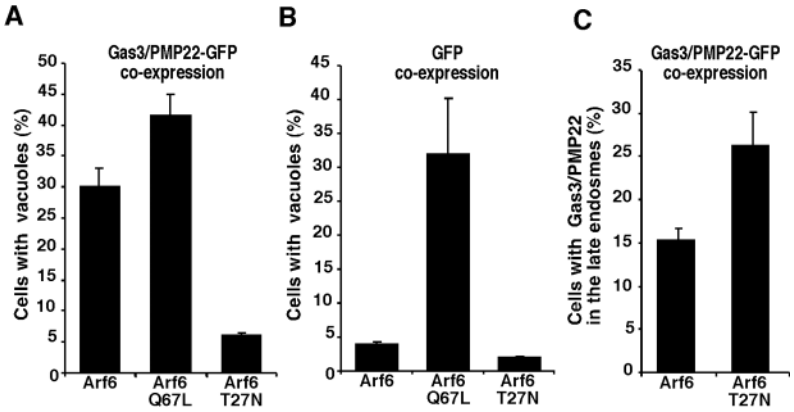

Fig. 9. Gas3/PMP22 requires Arf6 to induce membrane internalization. (A) Arf6, Arf6-Q67L and Arf6-T27N were co-expressed with Gas3/PMP22-GFP in NIH3T3 cells. After 18 hours from microinjection cells were fixed and processed for immunofluorescence to visualize Gas3/PMP22-GFP and Arf6. Cells were scored for accumulation of vacuoles double positive for Arf6 and Gas3/PMP22. Data represent arithmetic means±s.d. for four independent experiments. (B) Arf6, Arf6-Q67L and Arf6-T27N were co-expressed with PH-GFP in NIH3T3 cells. After 18 hours from microinjection cells were fixed and processed for immunofluorescence to visualize PH-GFP and Arf6. Cells were scored for accumulation of vacuoles. Data represent arithmetic means±s.d. for four independent experiments. (C) Arf6 and Arf6-T27N were co-expressed with Gas3/PMP22-GFP in NIH3T3 cells. After 18 hours from microinjection cells were fixed and processed for immunofluorescence to visualize Gas3/PMP22-GFP and LBPA. Cells were scored for accumulation vesicles double positive for Gas3/PMP22 and LBPA. Data represent arithmetic means ± s.d. for four independent experiments.

Gas3/PMP22, co-localization in the same vacuolar structures was observed. In addition, both Gas3/PMP22- and Arf6-Q67L-induced vacuoles were coated with actin, contained PIP_2 and accumulated MHC I. These results strongly suggest that Gas3/PMP22- and Arf6-Q67L-induced vacuoles represent the same endosomal compartment. This piece of evidence is also supported by the ability of the Arf6 dominant negative mutant T27N, which inhibits membrane recycling, to suppress Gas3/PMP22-induced vacuoles.

Two hypotheses could be formulated based on the reported data. Gas3/PMP22 could induce vacuole accumulation by locally increasing the GTP status of Arf6 at the PM, which in turn can bind and activate PIP 5-kinase, leading to elevated PIP_2 (Honda et al., 1999; Brown et al., 2001). Alternatively, Gas3/PMP22 could enter the Arf6 endosomal pathway and, if expressed at high levels, it could interfere with the recycle back to the PM, which would lead to the accumulation of PIP_2 endosomes that tether and fuse with one another forming large membrane vacuoles. It is clear that additional experiments are required to endorse one of the above-suggested models.

It is interesting to note that both cells expressing Gas3/PMP22 and activated Arf6 similarly show depletion of stress fibers and resist the formation of stress fibers induced by lysobiphosphatidic acid, as a consequence of RhoA inhibition (Brancolini et al., 1999; Boshans et al., 2000). Therefore, it might be possible that Gas3/PMP22 could induce stress fiber depletion, besides vacuole accumulation and PIP_2 increase, through Arf6 activation.

Gas3/PMP22 can regulate cell adhesion and apoptosis. Bcl-2 and Rho-kinase when co-expressed with Gas3/PMP22 can suppress its ability to induce cell death and changes in cell spreading, respectively (Brancolini et al., 1999). Gas3/PMP22 can induce vacuolar membrane when Bcl-2 and Rho-kinase were co-expressed. This implies that the effect on membrane traffic is not a consequence of a reduction from the adhesion substrate or of a vacuolization caused by cell death. However, it is possible that by interfering with PM recycle, Gas3/PMP22 could induce both cell death and alterations in cell adhesion. We have addressed this question by analyzing whether the dominant negative form of Arf6 could suppress the apoptotic and adhesion responses triggered by Gas3/PMP22. Unfortunately T27N has itself an effect on cell adhesion and spreading (Song et al., 1998) and on cell survival (Chies unpublished observation) that renders its use impossible.

The data presented here also indicate that not all vacuoles accumulating Gas3/PMP22 are positive for PIP_2 and actin. Co-localization studies have demonstrated that these vacuoles, negative for PIP_2 and actin were instead positive for LBPA, a marker of the late endosomes (Kobayashi et al., 1998).

Increased dosage of myelin proteolipid protein (PLP) in the central nervous system is, similarly to PMP22, involved in dysmyelinating disorders such as Pelizaeus-Merzbacher disease and spastic paraplegia (Garbern et al., 1999). Similarly to Gas3/PMP22, overexpressed PLP was routed to late endosomes, where it causes sequestration of cholesterol and mistrafficking of raft components (Simons et al., 1999). The recent discovery that also Gas3/PMP22 can associate with glycosphingolipid/cholesterol-enriched membranes domain (Erne et al., 2002; Hasse et al., 2002), encourages further investigations aimed at understanding whether Gas3/PMP22 could trigger mislocalization of raft components in the late endosome. However, we noticed that accumulation in the late endosomes could be observed also when claudin-15 was overexpressed, thus suggesting that this route could be common to different tetraspan proteins. By contrast, overexpression of claudin-15 was unable to trigger accumulation of annexin II and Arf6-positive vacuoles, thus reinforcing the specificity of the Gas3/PMP22 effect on the Arf6-regulated membrane traffic.

How could the effect of Gas3/PMP22 on membrane trafficking relate to myelin stability and CMT1A disease? In this respect it will be important to observe membrane vacuoles in vivo, by studies on CMT nerves. However, this type of analysis may not be simple to achieve since the disease is progressive and the secondary effects, such as the onion bulb formation, could mask primary effects caused by Gas3/PMP22 duplication (Hanemann and Muller, 1998). Interestingly accumulation of vacuoles of unknown origin has been described in SCs of transgenic rats overexpressing 16-30 copies of Gas3/PMP22 (Niemann et al., 2000). In this manuscript we have confirmed this observation and we have detected vacuoles, which sometimes resemble myelin figures, in cultured SCs from transgenic rats. Recently, intracellular vacuoles, which resemble myelin figures, have been observed also in cultured cells overexpressing Gas3/PMP22 (Dickson et al., 2002). In this study, accumulation of Gas3/PMP22 into two distinct

intracellular compartments can be observed: aggresomes and intracellular myelin-like figures (Dickson et al., 2002). Aggresome formation has also been hypothesized as a possible pathogenic mechanism responsible for Gas3/PMP22-related neuropathies (Ryan et al., 2002). Interestingly, intracellular myelin-like figures were immunoreactive to LAMP (lysosome-associated membrane protein), possibly as a consequence of autophagy, and aggresomes contained ubiquitinated PMP22, which suggests a common aim, in these structures, for degradation (Ryan et al., 2002; Dickson et al., 2002). We could not prove that, from the actin/PIP_2-positive pool of vacuoles, Gas3/PMP22 moved and accumulated in the late endosomes for degradation. In this context it will be interesting to study, in vivo, the movement/behaviour of the vacuoles containing Gas3/PMP22, and to understand whether autophagy or other mechanisms, such as ubiquitination, regulate the stability of the vacuoles. However, since the accumulation of Gas3/PMP22 in the late endosomes was observed also in cells overexpressing Arf6-T27N, it can be suggested that mislocalization/degradation of Gas3/PMP22 can also occur independently by Arf6.

In conclusion our studies indicate that overexpressed Gas3/PMP22 can accumulate in different intracellular membrane compartments and can alter membrane trafficking in cultured cells. Further in vivo experiments are required to unambiguously identify which traffic event is critical for triggering myelin instability and the CMT1A disease.

We thank Welfide Corporation (Osaka) for providing us with Y-27632; T. Leung and L. Lim (Singapore) for the expression plasmids encoding the different ROKα used; S. L. Schimd (La Jolla) for the expression plasmids encoding Dyn1 and Dyn1-K44A; J. Donaldson (Bethesda) for Arf6 constructs; I. de Curtis (Milano) for p95-APP1 constructs; and J. Gruenberg (Geneva) for anti-LBPA antibodies. L.N. and A.S. thank U. Suter (Zurich) and K. A. Nave (Heidelberg) for rats overexpressing Gas3/PMP22. We also thank M. Stebel (Trieste) for helping to prepare SCs; S. Marzinotto for experiments on REF cells; and E. di Centa (Udine) for claudin-15 construct and sequencing service. We are grateful to J. Donaldson (Bethesda), I. de Curtis (Milano) and F. Demarchi (Trieste) for critically reading the manuscript. This work was supported by Telethon-Progetto n.1188 and COFIN-2000 (MIUR) to C.B.

References

Altschuler, Y., Barbas, S. M., Terlecky, L. J., Tang, K., Hardy, S., Mostov, K. E. and Schmid, S. L. (1998). Redundant and distinct functions for dynamin-1 and dynamin-2 isoforms. *J. Cell Biol.* **143**, 1871-1881.

Attardi, L. D., Reczek, E. E., Cosmas, C., Demicco, E. G., McCurrach, M. E., Lowe, S. W. and Jacks, T. (2000). PERP, an apoptosis-associated target of p53, is a novel member of the PMP-22/gas3 family. *Genes and Dev.* **14**, 704-718.

Baechner, D., Liehr, T., Hameister, H., Altenberger, H., Grehl, H., Suter, U. and Rautenstrauss, B. (1995). Widespread expression of the peripheral myelin protein-22 gene (pmp22) in neural and non-neural tissue during murine development. *J. Neurosci. Res.* **42**, 733-741.

Bajno, L., Peng, X. R., Schreiber, A. D., Moore, H. P., Trimble, W. S. and Grinstein, S. (2000). Focal exocytosis of VAMP3-containing vesicles at sites of phagosome formation. *J. Cell Biol.* **149**, 697-706.

Boshans, R. L., Szanto, S., van Aelst, L. and D'Souza-Schorey, C. (2000). ADP-ribosylation factor 6 regulates actin cytoskeleton remodeling in coordination with Rac1 and RhoA. *Mol. Cell. Biol.* **20**, 3685-3694.

Brancolini, C., Marzinotto, S., Edomi, P., Agostoni, E., Fiorentini, C., Muller, H. W. and Schneider, C. (1999). Rho-dependent regulation of cell spreading by the tetraspan membrane protein Gas3/PMP22. *Mol. Biol. Cell* **10**, 2441-2459.

Brancolini, C., Edomi, P., Marzinotto, S. and Schneider, C. (2000). Exposure at the cell surface is required for Gas3/PMP22 to regulate both cell death and cell spreading: implication for the Charcot-Marie-Tooth type 1A and Dejerine-Sottas diseases. *Mol. Biol. Cell* **11**, 1-14.

Bronstein, J. M. (2000). Function of tetraspan proteins in the myelin sheath. *Curr. Opin. Neurobiol.* **10**, 552-557.

Brown, F. D., Rozelle, A. L., Yin, H. L., Balla, T. and Donaldson, J. G. (2001). Phosphatidylinositol 4,5-bisphosphate and Arf6-regulated membrane traffic. *J Cell Biol.* **154**, 1007-1017.

D'Urso, D., Brophy, P. J., Staugaitis, S. M., Gillespie, C. S., Frey, A. B., Stempak, J. G. and Colman, D. R. (1990). Protein zero of peripheral nerve myelin: biosynthesis, membrane insertion, amd evidence for homotypic interaction. *Neuron* **4**, 449-460.

Daro, E., van der Sluijs, P., Galli, T. and Mellman, I. (1996). Rab4 and cellulbrevin define different early endosome populations on the pathway of transferrin receptor recycling. *Proc. Natl. Acad. Sci. USA.* **93**, 9559-9564.

Di Cesare, A., Paris, S., Albertinazzi, C., Dariozzi, S., Andersen, J., Mann, M., Longhi, R. and de Curtis, I. (2000). p95-APP1 links membrane transport to Rac-mediated reorganization of actin. *Nat. Cell Biol.* **2**, 521-530.

Dickson, K. M., Bergeron, J. J. M., Shames, I., Colby, J., Nguyen, D. T., Chevet, E., Thomas, D. Y. and Snipes, G. J. (2002). Association of calnexin with mutant peripheral myelin protein-22 *ex vivo*: A basis for "gain-of-function" ER diseases. *Proc. Natl. Acad. Sci. USA.* **99**, 9852-9857.

Erne, B., Sansano, S., Frank, M. and Schaeren-Wiemers, N. (2002). Rafts in adult peripheral nerve myelin contain major structural myelin proteins and myelin and lymphocyte protein (MAL) and CD59 as specific markers. *J. Neurochem.* **82**, 550-562.

Fabbretti, E., Edomi, P., Brancolini, C. and Schneider, C. (1995). Apoptotic phenotype induced by overexpression of wild-type gas3/PMP22: its relation to the demyelinating peripheral neuropathy CMT1A. *Genes and Dev.* **9**, 1846-1856.

Garbern, J. Y., Cambi, F., Lewis, R., Shy, M., Sima, A., Kraft, G., Vallat, J. M., Bosch, E. P., Hodes, M. E., Dlouhy, S. et al. (1999). Peripheral neuropathy caused by proteolipid protein gene mutations. *Ann. NY Acad. Sci* **883**, 351-365.

Hall, A. (1998). Rho GTPases and the actin cytoskeleton. *Science* **279**, 509-514.

Hanemann, C. O. and Muller, H. W. (1998) Pathogenesis of Charcot-Marie-Tooth 1A (CMT1A) neuropathy. *Trends Neurosci.* **21**, 282-286.

Hasse, B., Bosse, F. and Muller, H. W. (2002). Proteins of peripheral myelin are associated with glycosphingolipid/cholesterol-enriched membranes. *J. Neurosci. Res.* **69**, 227-232.

Hinshaw, J. E. (2000). Dynamin and its role in membrane fission. *Annu. Rev. Cell. Dev. Biol.* **16**, 483-519.

Hirst, J. and Robinson, M. S. (1998). Clathrin and adaptors. *Biochim. Biophys. Acta* **1404**, 173-193.

Honda, A., Nogami, M., Yokozeki, T., Yamazaki, M., Nakamura, H., Watanabe, H., Kawamoto, K., Nakayama, K., Morris, A. J., Frohman, M. A. et al. (1999). Phosphatidylinositol 4-phosphate 5-kinase alpha is a downstream effector of the small G protein ARF6 in membrane ruffle formation. *Cell* **99**, 521-532.

Huxley, C., Passage, E., Manson, A., Putzu, G., Figurearella-Branger, D., Pellisier, J. and Fontes, M. (1996). Construction of a mouse model of Charcot-Marie-Tooth disease type 1A by pronuclear injection of human YAC DNA. *Hum. Genet.* **5**, 563-569.

Ishizaki, T., Naito, M., Fujisawa, K., Maekawa, M., Watanabe, N., Saito, Y. and Narumiya, S. (1997). p160ROCK, a Rho-associated coiled-coil forming protein kinase, works downstream of Rho and induces focal adhesions. *FEBS Lett.* **404**, 118-124.

Kobayashi, T., Stang, E., Fang, K. S., de Moerloose, P., Parton, R. G. and Gruenberg, J. (1998). A lipid associated with the antiphospholipid syndrome regulates endosome structure and function. *Nature* **392**, 193-197.

Leung, T., Chen, X. Q., Manser, E. and Lim, L. (1996). The p160 RhoA-binding kinase ROKα is a member of a kinase family and is involved in the reorganization of the cytoskeleton. *Mol. Cell. Biol.* **16**, 5313-5327.

Magyar, J. P., Martini, R., Ruelicke, T., Aguzzi, A., Adlkofer, K., Dembic, Z., Zielasek, J., Toyka, K. V. and Suter, U. (1996). Impaired differentiation of Schwann cells in transgenic mice with increased PMP22 gene dosage. *J. Neurosci.* **16**, 5351-5360.

Matafora, V., Paris, S., Dariozzi, S. and de Curtis, I. (2001). Molecular mechanisms regulating the subcellular localization pf p95-APP1 between the endosomal recycling compartment and sites of actin organization at the cell surface. *J. Cell Sci.* **114**, 4509-4520.

Matsui, T., Amano, M., Yamamoto,T., Chihara, K., Nakafuku, M., Ito, M., Nakano, T., Okawa, K., Iwamatsu, A. and Kaibuchi, K. (1996). Rho-associated kinase, a novel serine/threonine kinase, as a putative target for small GTP binding protein Rho. *EMBO J.* **15**, 2208-2216.

Mellman, I. (2000). Quo vadis: polarized membrane recycling in motility and phagocytosis. *J. Cell Biol.* **149**, 529-530.

Merrifield, C. J., Rescher, U., Almers, W., Proust, J., Gerke, V., Sechi, A. S. and Moss, S. E. (2001). Annexin 2 has an essential role in actin-based macropinocytic rocketing. *Curr. Biol.* **11**, 1136-1141.

Naef, R. and Suter, U. (1998). Many facets of the peripheral myelin protein PMP22 in myelination and disease. *Microsc. Res. Tech.* **41**, 359-371.

Naef, R. and Suter, U. (1999). Impaired intracellular trafficking is a common disease mechanism of PMP22 point mutations in peripheral neuropathies. *Neurobiol. Dis.* **6**, 1-14.

Niemann, S., Sereda, M. W., Suter, U., Griffiths, I. R. and Nave, K. A. (2000). Uncoupling of myelin assembly and Schwann cell differentiation by transgenic overexpression of peripheral myelin protein 22. *J. Neurosci.* **20**, 4120-4128.

Notterpek, L., Ryan, M. C., Tobler, A. R. and Shooter, E. M. (1999). PMP22 accumulation in aggresomes: implications for CMT1A pathology. *Neurobiol. Dis.* **6**, 450-460.

Notterpek, L., Roux, K. J., Amici, S. A., Yazdanpour, A., Rahner, C. and Fletcher, B. S. (2001). Peripheral myelin protein 22 is a constituent of intercellular junctions in epithelia. *Proc. Natl. Acad. Sci. USA* **98**, 14404-14409.

Palacios, F., Price, L., Schweitzer, J., Collard, J. G. and D'Souza-Schorey, C. (2001). An essential role for ARF6-regulated membrane traffic in adherens junction turnover and epithelial cell migration. *EMBO J.* **20**, 4973-4986.

Patel, I. P. and Lupski, J. R. (1994). Charcot-Marie-Tooth disease: a new paradigm for the mechanism of inherited disease. *Trends Genet.* **10**, 128-133.

Perea, J., Robertson, A., Tolmachova, T., Muddle, J., King, R. H., Ponsford, S., Thomas, P. K. and Huxley, C. (2001). Induced myelination and demyelination in a conditional mouse model of Charcot-Marie-Tooth disease type 1A. *Hum. Mol. Genet.* **10**, 1007-1018.

Peters, P. J., Hsu, V. W., Ooi, C. E., Finazzi, D., Teal, S. B., Oorschot, V., Donaldson, J. G. and Klausner, R. D. (1995). Overexpression of wild-type and mutant ARF1 and ARF6: distinct perturbations of nonoverlapping membrane compartments. *J. Cell Biol.* **128**, 1003-1017.

Radhakrishna, H. and Donaldson, J. G. (1997). ADP-ribosylation factor 6 regulates a novel plasma membrane recycling pathway. *J. Cell Biol.* **139**, 49-61.

Ren, M., Xu, G., Zeng, J., de Lemos-Chiarandini, C., Adesnik, M. and Sabatini, D. D. (1998). Hydrolysis of GTP on rab11 is required for the direct delivery of transferrin from the pericentriolar recycling compartment to the cell surface but not from sorting endosomes. *Proc. Natl. Acad. Sci. USA* **95**, 6187-6192.

Ridley, A. J. (2001). Rho proteins: linking signaling with membrane trafficking. *Traffic* **2**, 303-310.

Ryan, M. C., Shooter, E. M. and Notterpek, L. (2002). Aggresome formation in neuropathy models based on peripheral myelin protein 22 mutations. *Neurobiol Dis.* **10**, 109-118.

Sechi, A. S. and Wehland, J. (2000). The actin cytoskeleton and plasma membrane connection: PtdIns(4,5)P(2) influences cytoskeletal protein activity at the plasma membrane. *J. Cell. Sci.* **113**, 3685-3695.

Sereda, M., Griffiths, I., Puhlhofer, A., Stewart, H., Rossner, M. J., Zimmermann, F., Magyar, J. P., Schneider, A., Hund, E., Meinck, H. M. et al. (1996). A transgenic rat model of Charcot-Marie-Tooth disease. *Neuron* **16**, 1049-1060.

Simons, M., Kramer, E. M., Macchi, P., Rathke-Hartlieb, S., Trotter, J., Nave, K. A. and Schulz, J. B. (2002). Overexpression of the myelin proteolipid protein leads to accumulation of cholesterol and proteolipid protein in endosomes/lysosomes: implications for Pelizaeus-Merzbacher disease. *J. Cell Biol.* **157**, 327-336.

Snipes, G. J., Suter, U., Welcher, A. A. and Shooter, E. M. (1992). Characterization of a novel peripheral nervous system myelin protein (PMP22/SR13). *J. Cell Biol.* **117**, 225-238.

Song, J., Khachikian, Z., Radhakrishna, H. and Donaldson, J. G. (1998). Localization of endogenous ARF6 to sites of cortical actin rearrangement and involvement of ARF6 in cell spreading. *J. Cell. Sci.* **111**, 2257-2267.

Spreyer, P., Kuhn, G., Hanamann, C. O., Gillen, C., Schaal, H., Kuhn, R., Lemke, G. and Muller, H. W. (1991). Axon-regulated expression of a Schwann cell transcript that is homologous to a "growth arrest-specific" gene. *EMBO J.* **10**, 3661-3668.

Suter, U. and Snipes, J. C. (1995). Biology and genetics of hereditary motor and sensory neuropathies. *Annu. Rev. Neurosci.* **18**, 45-75.

Suter, U., Snipes, G. J., Schoener-Scott, R., Welcher, A. A., Pareek, S., Lupski, J. R., Murphy, R. A., Shooter, E. M. and Patel, P. I. (1994). Regulation of tissue-specific expression of alternative peripheral myelin protein-22 (PMP22) gene transcripts by two promoters. *J. Biol. Chem.* **269**, 25795-25808.

Tsukita, S., Furuse, M. and Itoh, M. (2001). Multifunctional strands in tight junctions. *Nat. Rev. Mol. Cell. Biol.* **2**, 285-289.

Turner, C. E. and Brown, M. C. (2001). Cell motility: ARNO and ARF6 at the cutting edge. *Curr. Biol.* **11**, R875-877.

Uehata, M., Ishizaki, T., Satoh, H., Ono, T., Kawahara, T., Morishita, T., Tamakawa, H., Yamagami, K., Inui, J., Maekawa, M. and Narumiya, S. (1997). Calcium sensitization of smooth muscle mediated by a Rho-associated protein kinase in hypertension. *Nature* **389**, 990-994.

Varnai, P. and Balla, T. (1998). Visualization of phosphoinositides that bind pleckstrin homology domains: calcium- and agonist-induced dynamic changes and relationship to myo-[3H]inositol-labeled phosphoinositide pools. *J. Cell Biol.* **143**, 501-510.

Welcher, A. A., Suter, U., de Leon, M., Snipes, G. J. and Shooter, E. M. (1991). A myelin protein is encoded by the homologue of a growth arrest-specific gene. *Proc. Natl. Acad. Sci. USA* **88**, 7195-7199.

Yamashiro, D. J., Tycko, B., Fluss, S. R. and Maxfield, F. R. (1984). Segregation of transferrin to a mildly acidic (pH 6.5) para-Golgi compartment in the recycling pathway. *Cell* **37**, 789-800.

Zoidl, G., Blass-Kampamann, S., D'Urso, D., Schmalenbach, C. and Muller, H. W. (1995). Retroviral-mediated gene transfer of the peripheral myelin protein PMP22 in Schwann cells: modulation of cell growth. *EMBO J.* **14**, 1122-1128.

Zoidl, G., D'Urso, D., Blass-Kampamann, S., Schmalenbach, C., Kuhn, R. and Muller, H. W. (1997). Influence of elevated expression of rat wild-type PMP22 and its mutant PMP22Trembler on cell growth of NIH3T3 fibroblasts. *Cell Tissue Res.* **287**, 459-470.